Surface & Coatings Technology 205 (2011) 3975–3986

Contents lists available at ScienceDirect

Surface & Coatings Technology

journal homepage: www.elsevier.com/locate/surfcoat

# Coating of hydroxyapatite films on metal substrates by seeded hydrothermal deposition

Dongxia Liu, Keith Savino, Matthew Z. Yates *

*Department of Chemical Engineering and Laboratory for Laser Energetics, University of Rochester, Rochester, NY, 14627, United States*

ARTICLE INFO

*Article history:*
Received 16 October 2010
Accepted in revised form 6 February 2011
Available online 21 March 2011

*Keywords:*
Crystallization
Hydrothermal
Hydroxyapatite
Electrochemical

ABSTRACT

Hydroxyapatite (HAP) was successfully coated on various metal substrates by a novel seeded hydrothermal deposition method. A nanoscale HAP seed layer was first formed by a short electrochemical synthesis. The seed layer promotes HAP crystal growth onto the surface during a subsequent hydrothermal crystallization step. The surface morphology and microstructure of the HAP coatings can be regulated by varying the reaction temperature, solution pH, calcium-to-phosphorus molar ratio in the starting solution, and hydrothermal deposition time. The new method has advantages over many other reported HAP deposition techniques in that it produces highly crystalline, crack-free, adherent films of uniform thickness. In all the films, the HAP crystals are preferentially oriented with the *c*-axis normal to the substrate. The as-developed HAP coatings are attractive for applications in the area of bioactive surface modification of metallic implants where the microstructure of the film is advantageous for promoting bone growth.



## 1. Introduction

The crystal structural and compositional similarity of hydroxyapatite ($Ca_{10}(PO_4)_6(OH)_2$, or HAP) with the hard tissues of vertebrates makes HAP attractive in orthopedic implants to accelerate bone growth around the implant [1]. However, HAP cannot be used clinically as a load bearing implant because of its poor mechanical properties [2]. Load bearing implants are typically formed from metals, such as stainless steel or titanium, that possess excellent mechanical properties but poor biocompatibility. As a result, a significant amount of research has focused on the development of methods to coat metal implants with thin films of HAP to improve biocompatibility while maintaining strong mechanical properties.

A variety of techniques have been developed for depositing HAP coatings on metal substrates, including thermal spraying, sputter coating, sol–gel coating, dip-coating, electrophoretic deposition, and electrochemical deposition [2–8]. Thermal spraying of HAP on implant devices has the advantage of high deposition rate and low cost [3,5]. However, poor coating–substrate adherence and non-uniform crystallinity of films deposited by thermal spraying reduce the lifetime of implants [3,9,10]. Sputter coating can generate HAP films with improved adherence to the substrates, but the coating process is high in cost and time-consuming [3,10].

Most of the reported HAP deposition techniques, including sputter coating, sol–gel coating, dip-coating, and electrophoretic deposition produce amorphous or poorly crystalline HAP films [6–8]. Highly crystalline HAP coatings are preferable because in vivo dissolution of the HAP film is reduced [3,11]. One approach to improve crystallinity of the deposited films is through high temperature sintering. The sintering step promotes crystallization of HAP, but usually causes film shrinkage and cracking due to either phase transformation of HAP or thermal expansion mismatch between the coatings and substrates [3,10]. Defects in the HAP films introduced during high temperature sintering can reduce device performance and lifetime.

One method that has been demonstrated to produce highly crystalline HAP films directly on a metal substrate is hydrothermal/electrochemical deposition [4,12–14]. In the electrochemical process, HAP is deposited on a metal cathode surface as a direct current is applied through a solution containing dissolved calcium and phosphate. The HAP crystals grow on the cathode surface as the applied electric current causes a local increase in pH due to electrolysis of water and an accumulation of $Ca^{2+}$ near the cathode due to electrostatic attraction. The main drawback of the electrochemical method is that electrolysis of water causes $H_2$ bubbles to form on the surface of the cathode. The gas bubbles obstruct the nucleation and growth of HAP crystals and can dislodge crystals already deposited. Therefore, dense and adherent HAP coatings are difficult to obtain in the electrochemical process. Some attempts have been made to evade $H_2$ production by adding either $H_2O_2$ or alcohols such as ethanol to the reactant solutions [15,16]. Hydrogen peroxide and ethanol reduce hydrogen gas evolution by changing the dominating electrochemical reactions to: $H_2O_2 + 2e = 2OH^-$ and $CH_3CH_2{-}OH + H_2O = CH_3CH_2O^- + H_3O^+$, but the results with these additives still show imperfect HAP films by electrodeposition.

* Corresponding author. Tel.: +1 585 273 2335; fax: +1 585 273 1348.
*E-mail address:* myates@che.rochester.edu (M.Z. Yates).

0257-8972/$ – see front matter © 2011 Elsevier B.V. All rights reserved.
doi:10.1016/j.surfcoat.2011.02.008

Large (micron sized) HAP crystals with excellent crystal quality can be produced by hydrothermal synthesis from aqueous solutions containing a calcium source and a phosphate source [17–19]. A calcium chelating agent is often added, usually a carboxylic acid such as acetic acid, lactic acid, citric acid, or ethylenediamine tetraacetic acid (EDTA), to control supersaturation of HAP and thus adjust the crystal growth rate. Upon heating the solution, the calcium carboxylate decomposes and calcium is slowly and continuously released into the solution. As the solution becomes supersaturated, calcium phosphate crystals nucleate and grow into larger sized crystals in the solution. One report attempted to grow HAP directly onto metal surfaces through hydrothermal synthesis, but poor surface coverage was obtained on titanium [20].

We recently reported a novel seeded hydrothermal deposition method for coating dense HAP films onto palladium to create high temperature proton conducting membranes [21]. Here we report a modified version of this synthetic approach that can be used to create uniform, highly crystalline coatings of HAP onto several metal substrates, including those typically used in orthopedic implants. Crystal seeds are first deposited by the electrochemical method for a very short period of time to avoid the film cracking caused by $H_2$ evolution. Subsequent hydrothermal crystal growth onto the seed layer produces a homogeneous and crack-free crystalline coating on the substrate. A series of experimental parameters were varied to adjust the HAP film thickness, surface morphology, microstructure and crystallinity. The method developed is practical for coating HAP over large surface areas and onto substrates of irregular geometry. With this new method, highly crystalline, dense, and adherent HAP films can be obtained.

## 2. Experimental

### 2.1. Materials

Analytical grade $Ca(NO_3)_2 \cdot 4H_2O$ (99.0% purity) and $(NH_4)_2HPO_4$ (>99.0% purity) were purchased from Alfa Aesar and EMD, respectively. $K_2HPO_4$ (99.99% purity), $CaCl_2 \cdot 2H_2O$ (99+% purity), NaCl (≥99.0% purity), tris(hydroxymethyl)-aminomethane (99.8+% purity), and disodium ethylenediaminetetraacetate dehydrate ($Na_2EDTA \cdot 2H_2O$) (ACS reagent, 99.0–101.0% purity) were all obtained from Sigma-Aldrich. 37% hydrochloride acid and 28.0–30.0% pure ammonium hydroxide were purchased from Mallinckrodt Chemicals. Titanium (Ti), stainless steel 316L (S/S316), copper (Cu), and aluminum (Al) plates (1.25 cm × 1.25 cm × 0.1 mm) were obtained from Small Parts, Inc. Deionized water was used for all the experiments.

### 2.2. Electrochemical deposition of HAP seeds

The metal substrates were polished with SiC sand paper (1500 grit), washed with an industrial soap solution, placed in ethanol/acetone (volume ratio = 50/50) solvent for 30 min in an ultrasonic cleaner, and then rinsed with deionized water. The cleaned metal substrate was used as the cathode and the anode was a platinum plate (25 mm × 25 mm × 127 μm). During the electrochemical reaction, the anode and cathode were held parallel to each other with a fixed distance of separation of 10 mm. The electrolyte solution was prepared as described in the literature, and consisted of 1.67 mM $K_2HPO_4$, 2.5 mM $CaCl_2$ and 138 mM NaCl in deionized water [4,22]. The solution was buffered to pH 7.2 using tris(hydroxymethyl)-

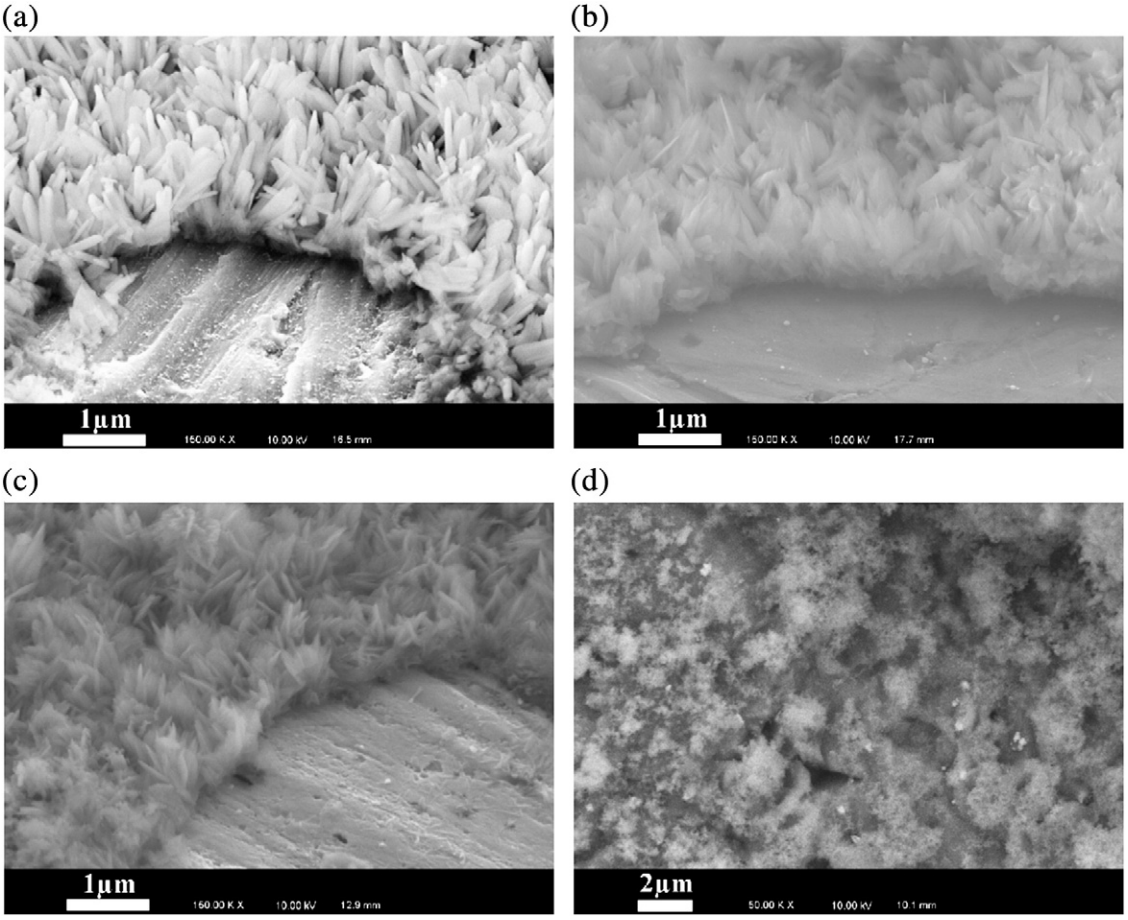


**Fig. 1.** Morphology of HAP seeds on titanium (a), S/S316 (b), copper (c), and aluminum (d) substrates grown by electrochemical deposition at 12.4 mA/cm$^2$ current for 2 min.

aminomethane and 37% hydrochloric acid. The anode and cathode were connected to a direct current power supply (Instek GPS-3030D) and immersed in the electrolyte solution. Electrochemical growth of the seed layer was carried out at 95 °C under constant current conditions. The metal substrate seeded with HAP crystals was then taken out of the electrolyte solution, rinsed with deionized water several times, and dried in air. The electrolyte solution had some visible turbidity and sediment after electrochemical deposition, indicating that some homogeneous nucleation of HAP in solution also occurred during electrochemical deposition.

### 2.3. Hydrothermal growth of HAP

In a typical hydrothermal synthesis, a solution of $Na_2EDTA$ (0.20 M) and $Ca(NO_3)_2$ (0.20 M) was prepared in 15 ml water and a solution of $(NH_4)_2HPO_4$ (0.12 M) in 15 ml water was prepared in a second container. The two source solutions were mixed together after pH of each solution was raised to 10.0 with ammonium hydroxide. The resulting combined solution was stirred at room temperature for about 20 min and then transferred to a Teflon-lined stainless steel pressure vessel (40 ml internal volume). The seeded substrate was submersed in the solution with the seed layer facing down and tilted ~45° relative to the bottom of the vessel. The seeded surface was facing down to avoid accumulation of sedimenting HAP crystals formed by homogeneous nucleation in solution during hydrothermal synthesis. The Teflon-lined vessel was placed in an oven for hydrothermal synthesis for 15 h at 200 °C and autogenous pressure. After cooling to room temperature in a fume hood, the sample was taken out, rinsed with deionized water several times, and dried in air.

### 2.4. Product characterization

Images of particle morphology and elemental analysis of the products were obtained using a field emission source scanning electron microscope (FESEM, Zeiss-Leo DSM982) equipped with an energy dispersive X-ray (EDX) spectrometer (EDAX Phoenix). The crystal structure of HAP was determined by X-ray powder diffraction (XRD) (Philips PW3020) with Cu Kα radiation (λ = 1.5418 Å) using an integration time of 2 h with a step size was 0.02°/3 s. The Fourier transform infrared (FTIR) spectrum was recorded with a spectrophotometer (FTIR-8400S Shimadzu) in the range of 500–2000 $cm^{-1}$ in attenuated total reflectance (ATR) mode using a diamond prism ATR stage. The sample was measured with 16 scans at an effective resolution of 1 $cm^{-1}$. SEM and XRD measurements were made directly on the as-deposited films. FTIR measurements were made on powder samples obtained by scratching off the films from the metal substrates.

## 3. Results and discussion

### 3.1. Seeding HAP on different substrates

Four kinds of metal plates (titanium, S/S316, copper and aluminum) were used as substrates for HAP seeding by electrochemical deposition. Fig. 1(a)–(d) shows the morphology of the seed layer that formed on the substrates in 2 min at 95 °C using a constant current density of 12.4 mA/$cm^2$. The seed layer is similar in morphology and microstructure on titanium, S/S316 and copper substrates, as illustrated in Fig. 1(a)–(c). The seed layer consists of platelet-shaped crystals with submicron width and length. XRD patterns of the seed layer on titanium, S/S316 and copper in Fig. 2(a) identify the materials as HAP crystals, formed most likely from plate-like octacalcium phosphate (OCP), a crystal phase that appears usually at low pH and certain temperature ranges in the electrochemical deposition of HAP [12]. Lower angle XRD measurements (not shown) reveal that none of the samples have any diffraction peaks from 2θ = 3° to 10°. The

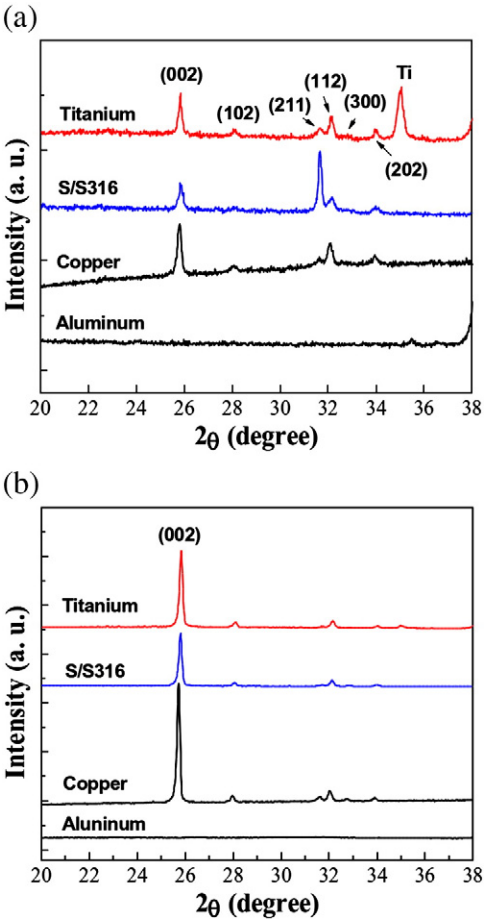


**Fig. 2.** XRD patterns of HAP (a) seeds by electrochemical deposition and (b) films by hydrothermal deposition on titanium, S/S316, copper and aluminum substrates.

absence of the characteristic OCP diffraction peak at 2θ = 4.7° indicates that HAP was the only crystalline phase detected in the electrochemically deposited samples [23]. The diffraction peak centered around 25.8° in Fig. 2(a) corresponds to the (002) plane of the HAP crystals. For randomly oriented HAP crystals, the standard intensity ratio of the (002) to the (300) plane is 0.67 (JCPDS No.86-0740). The intensity ratios of the (002) to the (300) plane in the XRD patterns shown in Fig. 2(a) are quite large in comparison with the standard ratio, which indicates a [002] (i.e. *c*-axis) is preferentially oriented normal to the metal substrates. If the crystals were all perfectly aligned with the *c*-axis normal to the substrate, the (002) diffraction peak would be the only one visible. The fact that several other HAP diffraction peaks are present in Fig. 2(a) indicates that some crystals are oriented in other directions. The sharp and strong XRD peaks of the seeds on titanium, S/S316, and copper denote a high degree of crystallization of deposited HAP.

The morphology and microstructure of the HAP seed layer deposited on aluminum are different from other substrates, as shown in Fig. 1(d). The seed layer contains some granular material, sparsely distributed on the substrate surface. The featureless XRD spectrum in Fig. 2(a) indicates that the granular material is amorphous or very poorly crystallized. The formation of such amorphous phase is possibly caused by $Al^{3+}$ ions released from the aluminum substrate. The strong alkaline conditions generated at the cathode in the electrochemical reaction cause $Al^{3+}$ ions from the surface to dissolve into the solution. The $Al^{3+}$ ions can react to potentially form amorphous aluminum phosphate, aluminum–calcium phosphate, and aluminum hydroxide. The smaller ionic radius of $Al^{3+}$ ions (0.51 Å)

compared to $Ca^{2+}$ (0.99 Å) disturbs the crystallization process [24]. The influence of $Al^{3+}$ on HAP crystallization is similar to that of $Mg^{2+}$ (ionic radius: 0.66 Å). It has been reported that incorporation of $Mg^{2+}$ into HAP reactant solutions decreases the HAP crystallinity by inhibiting growth of the (001) face of the crystals [25,26]. Since no crystalline phases were detectable by XRD, chemical analysis would

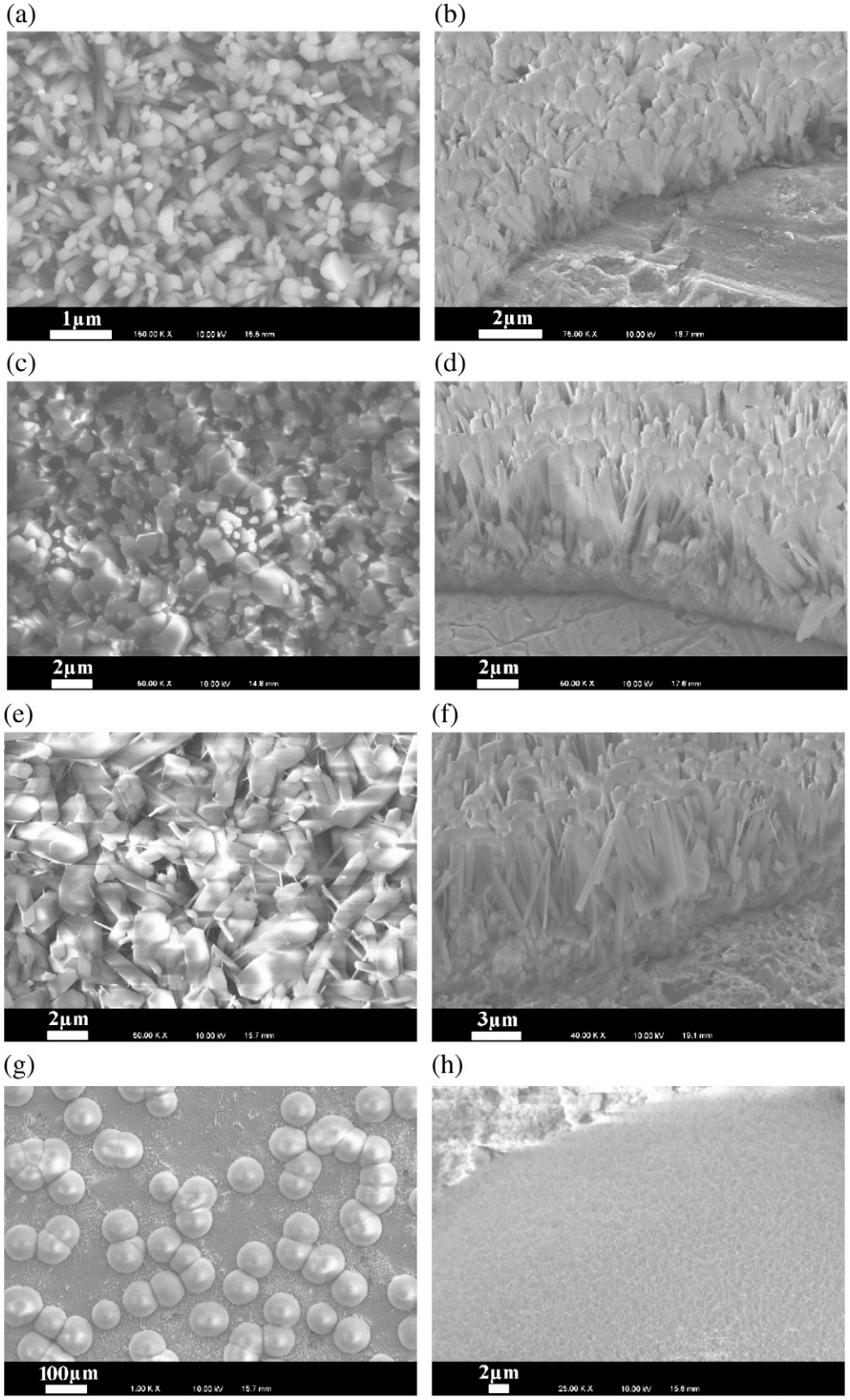


**Fig. 3.** Morphology of HAP coatings prepared by hydrothermal deposition at 200 °C for 15 h: (a) top-view image on titanium, (b) side-view image on titanium, (c) top-view image on S/S316, (d) side-view image on S/S316, (e) top-view image on copper, (f) side-view image on copper, (g) top-view image on aluminum, and (h) a higher magnified image of spherical particles in (g).

have to be done to determine the exact chemical composition of the amorphous phase shown in Fig. 1(d).

### 3.2. Hydrothermal growth of HAP on seeded substrates

The HAP seed layer formed by electrochemical deposition was used to promote hydrothermal growth of HAP coatings at the surface of the metal substrates. Seeded substrates similar to those shown in Fig. 1(a)–(d) were employed for hydrothermal growth under standard synthesis conditions described in the experimental section. Fig. 3(a)–(f) illustrates the surface and cross-sectional morphology of the HAP coatings grown on the titanium, S/S316 and copper substrates after the hydrothermal growth. The coatings exhibit a homogeneous porous coverage on all substrate surfaces and uniform thickness on each substrate. The crystals in the coatings are rod-like in shape, having a well-defined hexagonal crystal habit, as seen in Fig. 3(a), (c) and (e). The width of crystals grown from the titanium substrate (Fig. 3(a)) is less than 500 nm, while those from S/S316 and copper (Fig. 3(c) and (e)) are up to ~2 μm. The rod-shaped crystals are oriented perpendicular to the substrate, as shown in Fig. 3(b), (d) and (f). The crystals grown on titanium are shorter (~2 μm) than those on S/S316 and copper substrates (~7 μm and ~10 μm, respectively). A careful look at the substrate surfaces in Fig. 3 shows that the copper surface underlying the HAP layer became porous after hydrothermal deposition. The titanium and S/S316 surfaces, however, remained smooth after the deposition process. The porous copper surface was probably caused by corrosion of the substrate since the solution color changed from clear to shallow green after the reaction. The HAP layer on aluminum appears as spherical particles, as shown in Fig. 3(g). A higher magnified image of the spherical particles is shown in Fig. 3(h), indicating the HAP spheres are composed of many plate-like aggregates.

The XRD patterns of the HAP films after hydrothermal growth are shown in Fig. 2(b). The featureless XRD pattern of the HAP layer on aluminum indicates that it is amorphous, likely due to the incorporated $Al^{3+}$ ions interfering with crystal growth. For all other substrates, the diffraction peaks corresponding to HAP are obviously sharper and stronger compared to the crystals in the seed layer, which suggests a higher degree of HAP crystallization after the hydrothermal deposition. A strong enhancement in intensity of (002) diffraction peak compared to other peaks is observed in the patterns, which indicates that the *c*-axes of HAP crystals are dominantly oriented normal to the substrate, consistent with the SEM observation in Fig. 2(b), (d) and (f). The HAP crystal growth habit is consistent with surface crystallization of other hexagonal crystals. It is known that crystals tend to grow from seeded surfaces with the fastest growing axis (in this case, the *c*-axis) normal to the surface [27,28].

The elemental composition and functional group bands of the HAP coatings were studied with EDX and FTIR spectroscopy. The EDX and FTIR spectra of the coatings on titanium, S/S316 and copper are similar. As an example, Fig. 4(a)–(b) shows the EDX and FTIR spectra of HAP coatings formed on the titanium substrate. The spectrum in Fig. 4(a) is comprised of O, P and Ca peaks, confirming the presence of HAP. The C peak is most likely from the carbon tape used for the SEM observation. The HAP also contains a very small amount of carbon, possibly from the EDTA used during synthesis. External analysis (Midwest Microlab, LLC) of one representative HAP sample showed a carbon content of 0.8%. The semiquantitative analysis of EDX spectrum shows the calcium-to-phosphorus (Ca/P) atomic ratio is around 1.58, a little lower than the ideal stoichiometric value of 1.67. The nonstoichimetry (Ca deficiency) of HAP is consistent with reports from the literature for hydrothermal synthesis of HAP crystals [18,19]. The FTIR spectrum of HAP film given in Fig. 4(b) shows all absorption bands characteristic for HAP [18,29]. For $PO_4^{3-}$ groups, the $\nu_1$ vibration (symmetric stretching) is centered at 961 $cm^{-1}$, $\nu_3$ vibration (asymmetric stretching) occurs at 1088 and 1022 $cm^{-1}$, while $\nu_4$

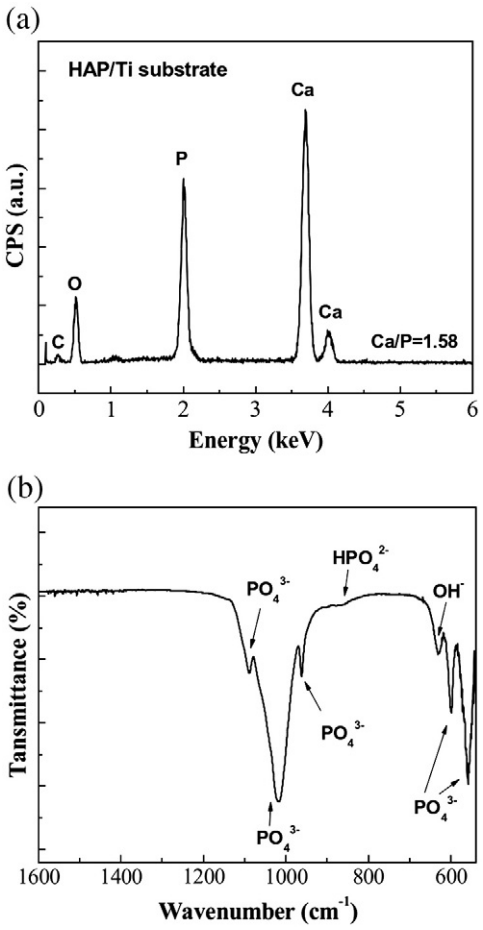


**Fig. 4.** EDX (a) and FTIR (b) spectra of HAP coatings prepared by seeded hydrothermal deposition.

vibration (asymmetric bending) is located at 602, 580, and 562 $cm^{-1}$. The librational vibration of $OH^-$ groups appears at 631 $cm^{-1}$. The absence of any distinct bands in the range of 1400–1500 $cm^{-1}$ indicates that HAP does not contain large quantities of carbonate ions. The band observed at 870 $cm^{-1}$ is ascribed to the $HPO_4^{2-}$ groups, in agreement with data reported in the literature [18,29]. The presence of $HPO_4^{2-}$ groups is consistent with the low Ca/P ratio in the synthesized HAP crystalline films. The absorption peaks due to $PO_4^{3-}$ showed stronger intensities and split cleanly, indicating a higher crystallinity of HAP coatings on the substrates [4].

Homogenous HAP coatings on the seeded metal substrates are formed through slow release of the calcium ions into the reactant solution, which is driven by the calcium-chelate decomposition [18,19]. The concentration of the calcium ions is controlled by the chelating agent so that the degree of supersaturation of the solution is constantly low in the deposition process. The lower degree of supersaturation generally causes heterogeneous nucleation and growth of the crystals to dominate [28]. As a result, HAP progressively nucleates and grows from the seeds at the substrate surfaces and finally converts into a uniform coating. The results show that the seeded hydrothermal deposition can coat HAP films on corrosion resistant metal substrates such as titanium and S/S316 commonly used in orthopedic implants. The resulting HAP coatings also contain desirable morphology and microstructure for biomedical applications. The porosity in the HAP coatings allows for ingrowth of tissues and enhanced fixation of implants [14]. Rod-like HAP crystals have been shown to enhance bonding between implants and bone at the early stages after implantation [30]. The *c*-axis orientation of HAP crystals in the films may improve bone growth if polarized under an electric

field. It is reported that dipole moment of lattice $OH^-$ ions are aligned in HAP at high temperatures under an applied electric field, which causes the crystals to be polarized along the *c*-axis. Cell proliferation and adhesion are enhanced at negatively charged HAP surfaces, and as a result accelerate bone-like crystal growth [31,32]. The HAP films developed by this method have crystal domains aligned in the *c*-axis direction so that they are expected to have stronger polarization under electric field to benefit bone growth.

To further our understanding of seeded hydrothermal deposition for coating HAP onto the metal substrates, a series of experiments were conducted to investigate the influence of various experimental parameters on the HAP coatings. In this series of experiments, the experimental conditions used for synthesis of HAP coatings in Fig. 3 were used as the base case for comparison. Individual experimental variables were changed and the effects of changing these variables were investigated by comparing the product to that obtained with the standard conditions. Unless otherwise noted, titanium was used as the substrate for HAP coatings in the following studies.

### 3.3. Effect of seed layer

To investigate the effect of the seed layer on the growth of HAP coatings, control experiments using unseeded metal substrates were performed. Fig. 5(a)–(c) shows the morphology of the HAP coatings formed on the titanium, S/S316 and copper substrates in sequence. No uniform coating is observed on the titanium substrate after the hydrothermal deposition, and only a few granular HAP particles (white dots in Fig. 5(a)) are scattered at the surface. The HAP coating on S/S316 substrate in Fig. 5(b) is similar to that on titanium substrate except that a few more HAP particles are at the substrate surface and the particles are clearly hexagonal in shape. The absence of the seed layer provides no nucleation sites for hydrothermal growth of HAP onto the substrates. The HAP particles scattered on the titanium and S/S316 substrates seem to grow from the surface flaws formed by polishing in the substrate cleaning process. Unlike titanium and S/S316 substrates, the HAP coating successfully grows on the unseeded copper substrate, as shown in Fig. 5(c). The HAP coating is dense and uniform, similar to that obtained on the seeded copper substrate in Fig. 3(e). It has been observed that the reactant solution etches the copper substrate by forming a porous surface after the hydrothermal deposition. The etched pits in the surface may act as nucleation sites for HAP growth. A similar study using iron substrates to grow HAP film in an acidic solution showed that the dissolved iron in the initial stage of the reaction resulted in the formation of nuclei for precipitation of HAP [20]. The inertness of titanium and S/S316 substrates to the reactant solution keeps the surface relatively smooth and prevents uniform HAP coatings. The study indicates that the seed layer is an important parameter for deposition of uniform HAP coatings onto substrates such as titanium and S/S316, but suggests improved surface nucleation will occur on rough surfaces.

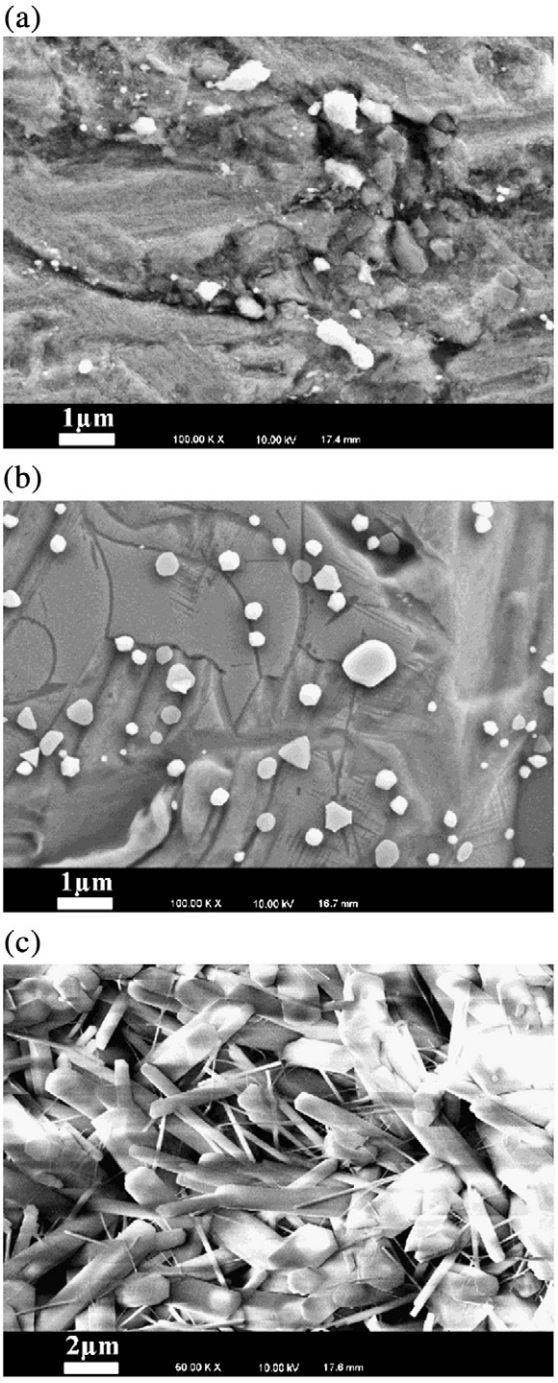


**Fig. 5.** Morphology of HAP films grown from unseeded titanium (a), S/S316 (b), and copper (c) substrates at 200 °C for 15 h.

### 3.4. Effect of hydrothermal deposition temperature

For the study of the hydrothermal deposition temperature effect, all of the HAP coatings were prepared under the standard deposition conditions on titanium except that the temperature was varied to 160 °C, 180 °C, and 220 °C. Fig. 6(a)–(f) shows the top-view and side-view morphology of HAP coatings grown under different reaction temperatures. The coatings become denser with an increase in temperature, which is indicated by the reduced size of gaps among crystals, as visualized from the top-view SEM images in Fig. 6(a), (c), and (e). The amount of HAP material deposited on the substrates increases with temperature as the width of crystals in the coatings increases remarkably. Needle-like crystals with a width of ~100 nm form at 160 °C, while rod-like crystals with widths up to 1 μm are observed after deposition at 220 °C. The side-view SEM images shown in Fig. 6(b), (d), and (f) are consistent with the top-view observation on crystal width changes. The side-view images also show that the crystal length increases slightly with decreasing temperature.

The hydrothermal growth of HAP coatings is based on the thermal decomposition of calcium chelate complex: $Ca\text{-}EDTA \leftrightarrow Ca^{2+} + EDTA^{2-}$. Temperature is a critical factor influencing the equilibrium in the deposition process. Under higher temperature conditions, the equilibrium shifts to the right hand side of the equation so that more calcium ions are released from the chelating complex for the HAP precipitation [18]. In addition, the solubility of HAP decreases with increasing temperature [33,34]. As a result, a higher amount of HAP material is coated onto the underlying substrates. The higher

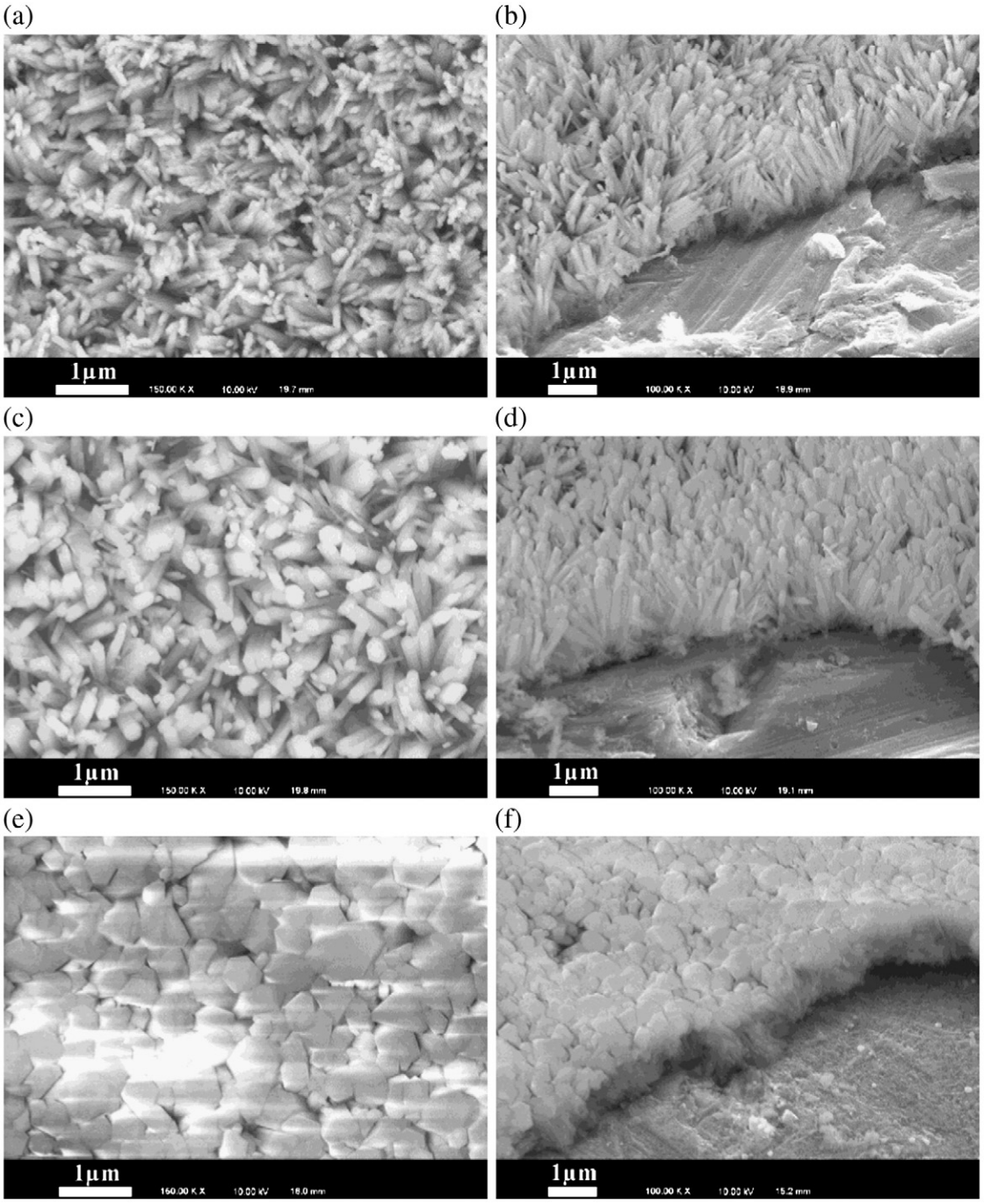


**Fig. 6.** HAP coatings as a function of synthesis temperature in the hydrothermal reactions: (a) top-view image, 160 °C, (b) side-view image, 160 °C, (c) top-view images, 180 °C, (d) side-view image, 180 °C, (e) top-view image, 220 °C, and (f) side-view image, 220 °C.

deposition temperature also increases the diffusion rate, which brings more reactants to the side-surfaces of the HAP crystals in the seed layer. As a result, the growth rate along the *a*-axis (perpendicular to the *c*-axis) is enhanced so that HAP crystals grow wider and the coatings get denser. At lower temperatures, lower $Ca^{2+}$ concentration and reduced diffusion causes the end-surfaces of the crystals to grow relatively faster than the sides so that the crystals grow longer and thinner. A further decrease in deposition temperature is restricted because of the slow decomposition rate of the calcium complexes. The higher reaction temperature is desired for calcium-chelate decomposition and HAP precipitation. However, the upper temperature limit is ~220 °C, above which the EDTA decomposes and results in carbonate apatites [18].

### 3.5. Effect of solution pH

Fig. 7(a)–(f) shows the influence of solution pH on the HAP coatings on titanium. The hydrothermal growth conditions were kept the same as the standard except the solution pH was adjusted to 8, 9, and 11. As seen in Fig. 7(a)–(f), increasing solution pH results in less HAP coating the substrates. The HAP crystal size (in terms of width and length) also decreases with increasing solution pH. Fig. 7(a)–(b) shows that the HAP particles in the coating had a size of ~1 μm in width and 5 μm in length when pH was 8. As pH was increased to 9, the width of the HAP particles decreased slightly but the length was reduced to ~3 μm. When pH was increased to 10, the particles had a width of ~500 nm and a length of ~2 μm (SEM images

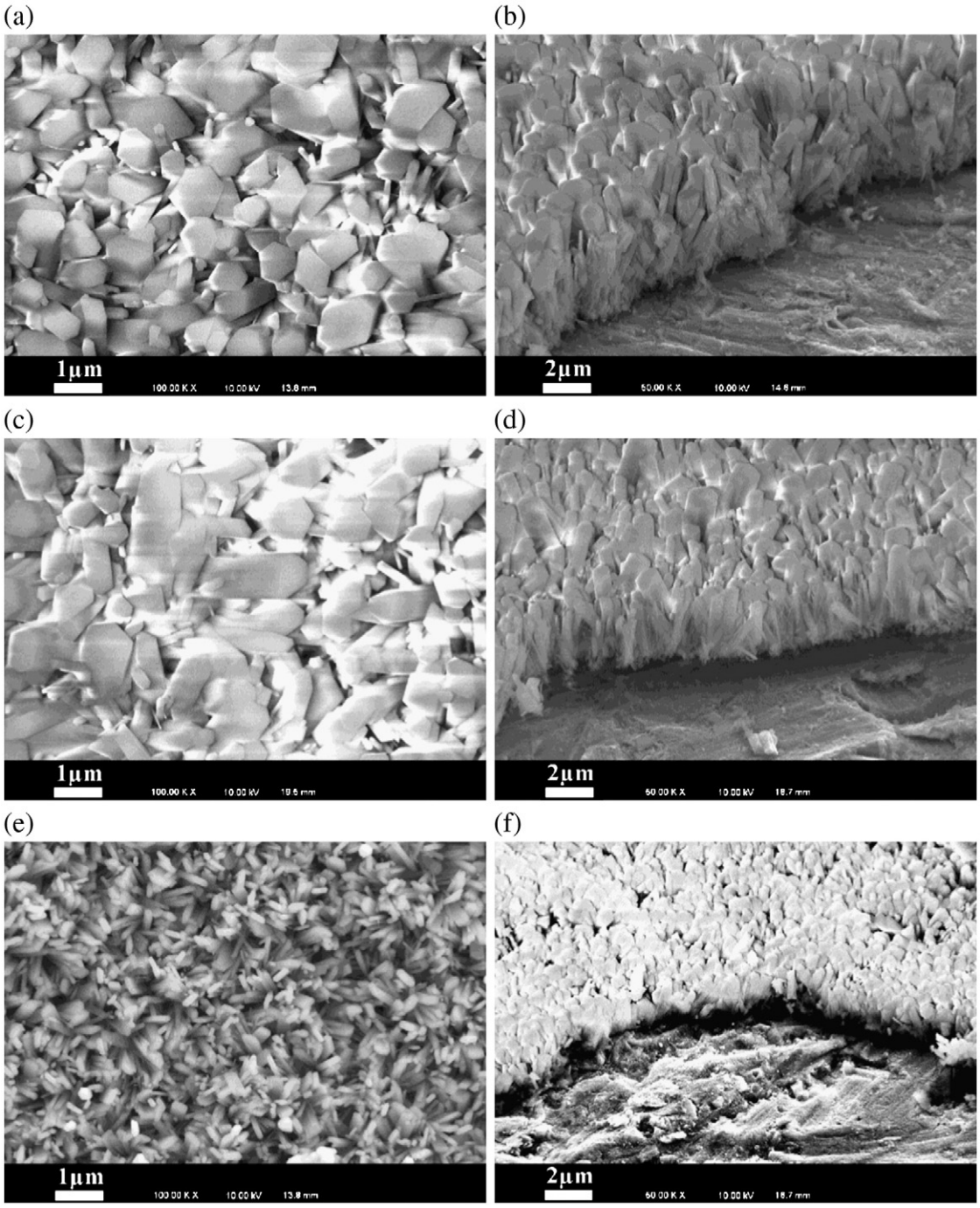


**Fig. 7.** HAP coatings on titanium as a function of pH of the reactant solutions: (a) top-view image, pH 8, (b) side-view image, pH 8, (c) top-view image, pH 9, (d) side-view image, pH 9, (e) top-view image, pH 11, and (f) side-view image, pH 11.

in Fig. 3(a)–(b)). Further increase of pH to 11 caused a decrease in the width to ~200 nm and length down to ~1.5 μm, as shown in Fig. 7(e)–(f).

The observations of changes in film morphology with changing pH can be understood by considering the solubility of HAP as a function of pH, as well as the kinetics of the reaction for forming HAP: $10Ca^{2+} + 6PO_4^{3-} + 2OH^- \leftrightarrow Ca_{10}(PO_4)_6(OH)_2$. Both of these factors affect the level of supersaturation and the competition between homogeneous nucleation in solution versus heterogeneous deposition and growth of the film on the surface [35,36]. As pH is lowered, the concentration of $OH^-$ ions is reduced so that the solution is under a lower level of supersaturation. Heterogeneous nucleation and growth of HAP dominate and the seed crystals grow larger. Increasing pH increases $OH^-$ concentration and as a result increases supersaturation of HAP. Homogeneous nucleation and growth of crystals dominate at higher supersaturation. The competition of homogeneous nucleation and growth in the reactant solution reduces the amount of HAP grown onto the seed layer. Therefore, thin and less dense HAP coatings are obtained at higher pH. The study shows that a lower solution pH is favorable for growing denser HAP coatings. However, very low pH can dissolve the HAP seed crystals or transform HAP to other calcium phosphate phases. It is known that monetite ($CaHPO_4$) is the stable phase of calcium phosphate at pH below ~5.0 [37].

### 3.6. Effect of Ca/P ratio in the reactant solutions

In the standard synthesis conditions, the molar ratio of calcium to phosphorous (Ca/P) was set equal to the stoichiometric ratio of 10/6. The effect of varying Ca/P molar ratio on the crystal growth on titanium was investigated by keeping the calcium ion concentration fixed, while adjusting the phosphate concentration to give Ca/P molar ratios of 10/3 and 10/10. As shown in Fig. 8(a), when the Ca/P ratio was 10/3, the particle width and length in the deposited HAP films are around 800 nm and 2 μm, respectively. As Ca/P ratio was changed to 10/10 in Fig. 8(b), the crystals in the coatings become thinner (~400 nm in width) and longer (~3 μm). For crystal grown under the standard conditions with a Ca/P ratio of 10/6, shown in Fig. 3(a)–(b), both crystal width and length have intermediate values between those with Ca/P ratios of 10/3 and 10/10.

The morphological changes of HAP coatings with varying Ca/P ratios (or, phosphate concentrations) are also related to the precipitation equilibrium: $10Ca^{2+} + 6PO_4^{3-} + 2OH^- \leftrightarrow Ca_{10}(PO_4)_6(OH)_2$. A decreasing phosphate amount reduces the degree of solution supersaturation so that heterogeneous nucleation and growth dominate and HAP grows preferably from the seed layer. Increasing phosphate ions in the solution increases the degree of supersaturation so that homogeneous nucleation and growth occur in solution and the amount of HAP deposited onto the seed layer is reduced. The morphological changes in the HAP coatings at different Ca/P molar ratios may also result from other possible mechanisms. A study of fluorohydroxyapatite crystallization using a double diffusion apparatus to control the concentration of calcium ions at one side of the apparatus and concentration of phosphate ions at the opposite side shows that HAP spheres were formed under calcium-rich conditions and hexagonal prisms under phosphate-rich conditions [38]. A more detailed study should be conducted to examine the crystal growth mechanism under variable reactant concentrations.

### 3.7. Effect of hydrothermal deposition time

The hydrothermal growth time was varied from 5 h, 10 h, and 25 h to examine the effect on the HAP coatings on titanium. As shown in Fig. 9(a)–(d), HAP crystals deposited in 5 h (Fig. 9(a)–(b)) are smaller in width and length compared to those in 10 h (Fig. 9(c)–(d)). A further increase of the reaction time to 15 h, which was employed in the standard reaction conditions, does not result in an obvious increase in HAP crystal size. A similar result was obtained when the reaction time was extended to 25 h (data not shown). The results show that the hydrothermal deposition of HAP is faster in the initial stage of the reaction, while the deposition slows down with increasing reaction time. It can be easily understood that sufficient amount of reactants are available in the beginning of the reaction so that the HAP deposition is fast. The consumption of the reactants reduces the concentrations of the calcium and phosphate ions and the reaction slows down or even stops after a period of time.

For applications requiring thick HAP coatings, a replacement of the reactant solution after the reactants are consumed can allow continued crystal growth. This approach to increasing HAP coating thickness was examined by repeating the hydrothermal growth step. After each growth step, the sample was taken out, rinsed with

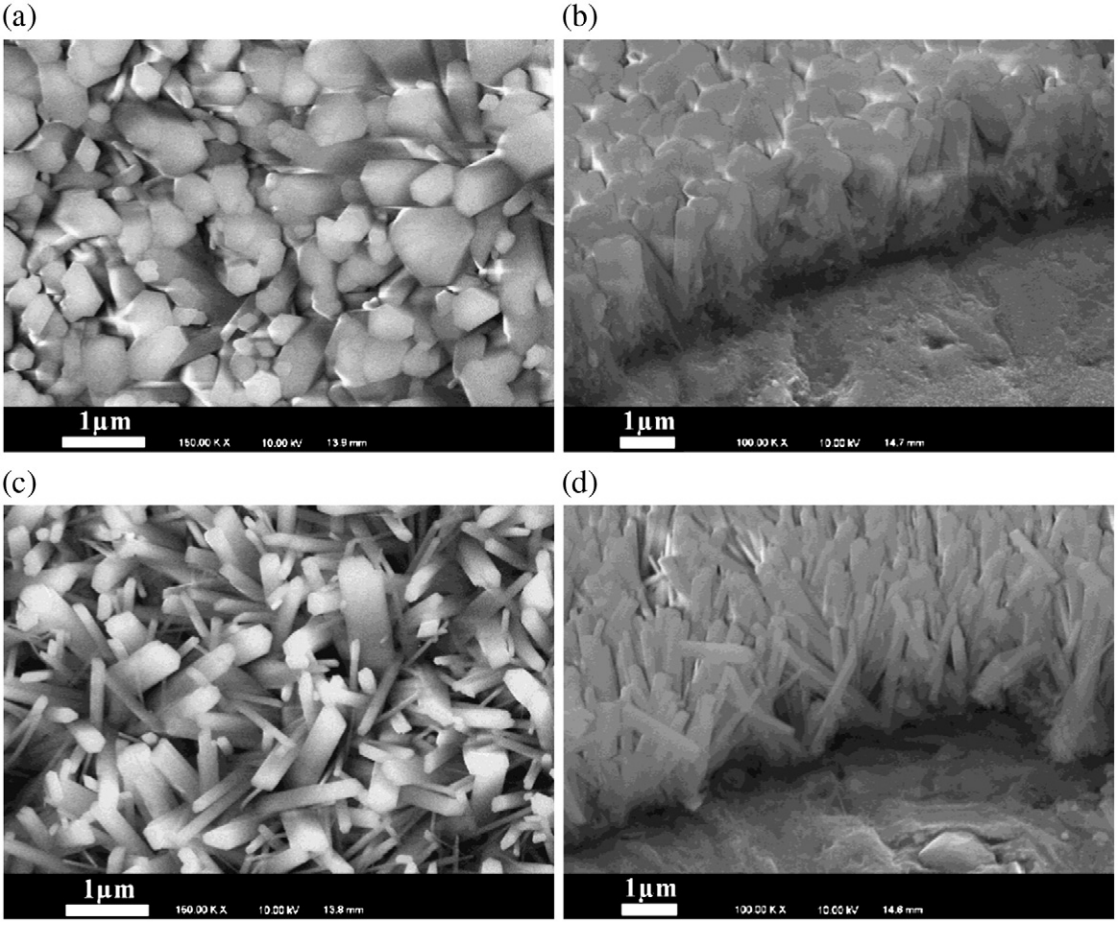


**Fig. 8.** HAP coatings on titanium as a function of Ca/P molar ratio in the reactant solutions: (a) top-view image, Ca/P = 10/3, (b) side-view image, Ca/P = 10/3, (c) top-view image, Ca/P = 10/10, and (d) side-view image, Ca/P = 10/10.

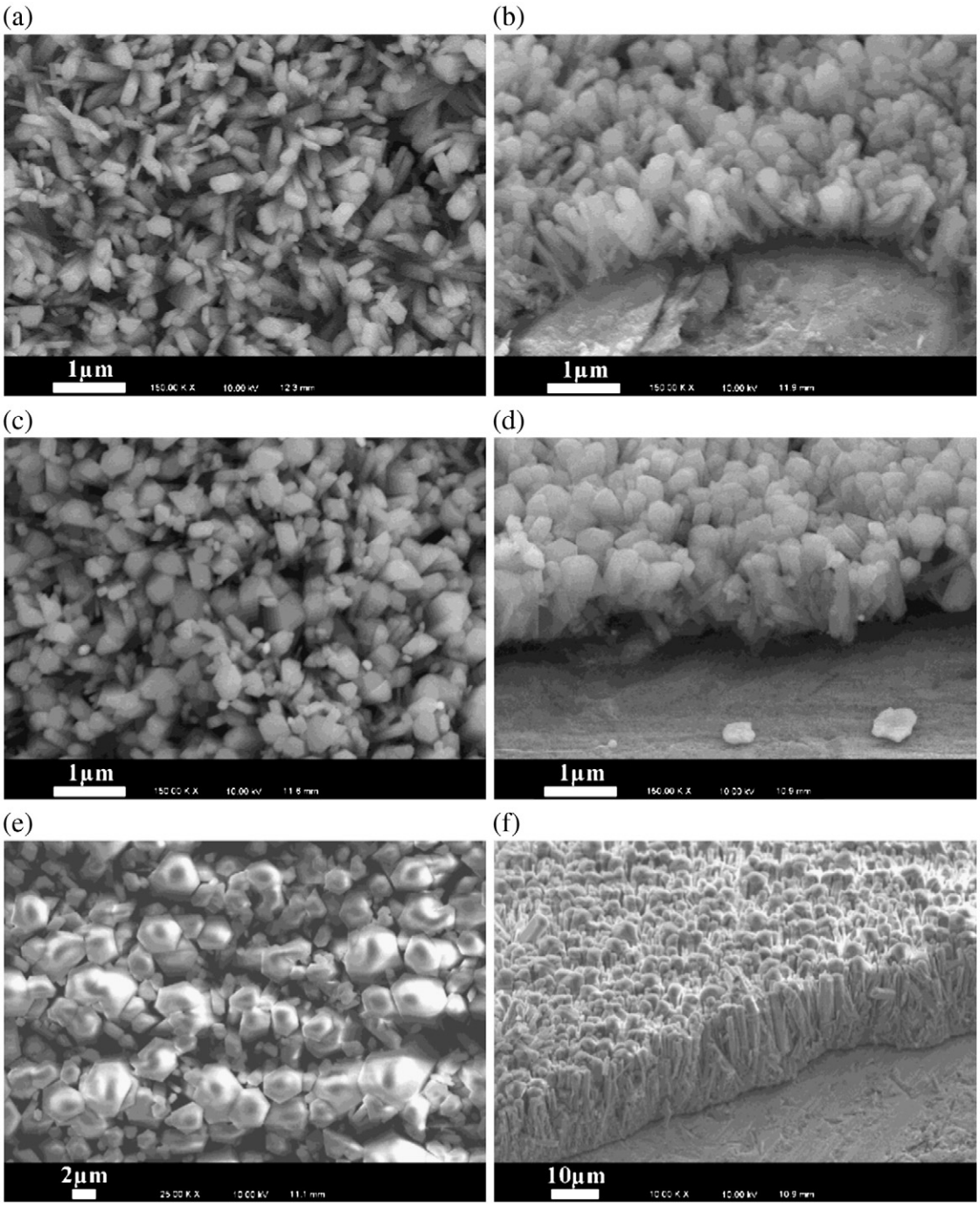


**Fig. 9.** HAP coatings on titanium as a function of hydrothermal reaction time: (a) top-view image, 5 h, (b) side-view image, 5 h, (c) top-view image, 10 h, (d) side-view image, 10 h, (e) top-view image, 60 h, and (f) side-view image, 220 °C, 60 h. (To keep sufficient calcium and phosphate sources in the reaction, the solution was replaced after every 15 h.)

deionized water and then placed into a new reactant solution to resume the hydrothermal solution. Fig. 9(e)–(f) shows that the HAP coating thickness is significantly increased. The coating is also obviously dense and uniform after such a long period (60 h in total) of hydrothermal deposition. The crystals in the coating have a typical width of ~4 μm and length ~25 μm.

### 3.8. Integrity of HAP films on metal substrate

A uniform, integral and crack-free coating of HAP is always desired in biomedical implants to enhance the coating-implant adherence. The HAP coatings produced by the seeded hydrothermal deposition promisingly meet the criteria. As an example, the low magnification SEM images in Fig. 10(a)–(b) show the integral morphology of the HAP coatings deposited under the standard synthesis conditions. The HAP coatings are dense, uniform and without any observable holes or cracks. Higher magnification images of the HAP coating shown in Fig. 3(a)–(b) appear similar to those prepared using the hydrothermal–electrochemical method [4]. However, cracks and holes in the coatings cannot be avoided in the electrochemical process over long growth times. As a comparison, an experiment using electrochemical deposition to grow HAP coatings for 30 min showed that serious cracks formed in the coatings, as seen in Fig. 10(c). A higher magnified SEM image (Fig. 10(d)) of the film shows that some

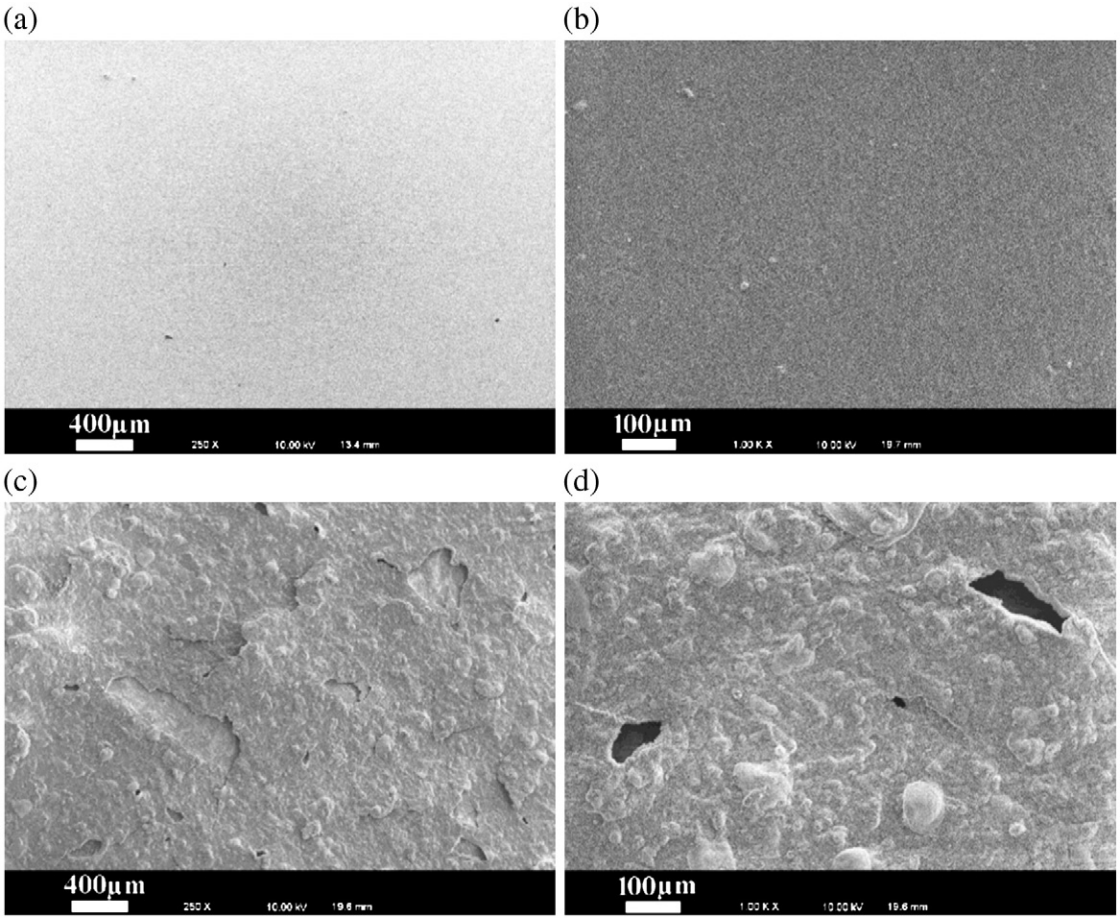


**Fig. 10.** Integrity of the HAP coatings prepared by seeded hydrothermal deposition (a) and (b) compared to coatings generated by electrochemical deposition at the seeding conditions for 30 min (c) and (d).

holes even exist in the coating area where no cracks appear. These cracks and holes in the coating are due to hydrogen bubbles dislodging crystals from the surface during electrochemical synthesis as a result of electrolysis of water. The key advantage of the present method is that electrochemical deposition is only carried out for a very short time to seed the surface with crystals. The subsequent hydrothermal growth onto the seeds completely avoids the hydrogen evolution problem to allow the HAP layer to grow as a dense film.

Crystallinity is another concern on the HAP coatings for implantation application since low crystallinity accelerates the speed of dissolution of the HAP film in the living body, causing the disappearance of coatings that bond to bone tissue at an early stage after implantation [3,11]. The HAP coatings produced by the seeded hydrothermal deposition are well and uniformly crystallized, as confirmed with XRD and FTIR analyses. High crystallinity is another advantage of the present method over most of the other coating approaches such as sol–gel coating, dip coating, thermal spraying, and sputter coating. The seeded hydrothermal deposition is also applicable to substrates with complex shapes or surface geometries so that little restrictions on implant shapes are required in the coating process.

## 4. Conclusions

HAP was coated on titanium, stainless steel, and copper by a seeded hydrothermal deposition method. The deposition includes an electrochemical reaction to form a thin layer of HAP seed crystals in a short period of time. Hydrothermal crystal growth from the seed layer results in dense and durable HAP films. By varying the synthesis parameters such as reaction temperature, solution pH, reaction time, and composition of the reactants, HAP coatings with desired surface morphology and microstructure can be easily achieved. The HAP coatings developed by the seeded hydrothermal deposition method show uniform thickness, structural integrity and higher crystallinity, which overcome one or several drawbacks facing most of the previous coating methods. The as-prepared HAP coatings are promising for applications in the area of bioactive surface modification for metal implants. The technique should be easily extended to metal substrates of varying shapes, such as mesh, porous, or tubular geometry.

## Acknowledgments

We acknowledge the DOE (DE-FG02-05ER15722), NSF CMMI-0856128, and the DOE through the Laboratory for Laser Energetics (DE-FC03-92SF19460) for financial support.

## References

[1] W. Suchanek, M. Yoshimura, J. Mater. Res. 13 (1998) 94.
[2] V. Nelea, C. Morosanu, M. Iliescu, I.N. Mihailescu, Appl. Surf. Sci. 228 (2004) 346.
[3] Y. Yang, K.-H. Kim, J.L. Ong, Biomaterials 26 (2005) 327.
[4] S. Ban, S. Maruno, J. Biomed. Mater. Res. 42 (1998) 387.
[5] P. Cheang, K.A. Khor, J. Mater. Process. Technol. 48 (1995) 429.
[6] D.-M. Liu, Q. Yang, T. Troczynski, Biomaterials 23 (1996) 691.
[7] A. Onder, E.-A. Osman, A. Sabri, Surf. Coat. Technol. 202 (2008) 2482.
[8] B. Aksakal, C. Hanyaloglu, J. Mater. Sci. Mater. Med. 19 (2008) 2097.
[9] K.A. Gross, C.C. Berndt, H. Herman, J. Biomed. Mater. Res. 39 (1998) 407.
[10] M. Hamdi, S. Hakamata, A.M. Ektessabi, Thin Solid Films 377–378 (2000) 484.
[11] W. Xue, S. Tao, X. Liu, X. Zheng, C. Ding, Biomaterials 25 (2004) 415.
[12] S. Ban, S. Maruno, Biomaterials 19 (1998) 1245.

[13] P. Peng, S. Kumar, N.H. Voelcker, E. Szili, R.S.C. Smart, H.J. Griesser, J. Biomed. Mater. Res. A 76 (2006) 347.
[14] N. Eliaz, M. Eliyahu, J. Biomed. Mater. Res. A 80 (2007) 621.
[15] Z. Zhao, H. Li, P. Sun, Y. Li, G. Huo, O. Masazumi, I. Ryoichi, Rare Met. Cemented Carbides 30 (2002) 6.
[16] J.-S. Chen, H.-Y. Juang, M.-H. Hon, J. Mater. Sci. Mater. Med. 9 (1998) 297.
[17] R.K. Roeder, G.L. Converse, H. Leng, W. Yue, J. Am. Ceram. Soc. 89 (2006) 2096.
[18] M. Andres-Verges, C. Fernandez-Gonzalez, M. Martinez-Gallego, J. Eur. Ceram. Soc. 18 (1998) 1245.
[19] W. Suchanek, H. Suda, M. Yashima, M. Kakihana, M. Yoshimura, J. Mater. Res. 10 (1995) 521.
[20] Y. Fujishiro, T. Sato, A. Okuwaki, J. Mater. Sci. Mater. Med. 6 (1995) 172.
[21] D. Liu, K. Savino, M.Z. Yates, Adv. Funct. Mater. 19 (2009) 3941.
[22] S. Ban, J. Hasegawa, Biomaterials 23 (2002) 2965.
[23] M. Kamitakahara, N. Ito, S. Murakami, N. Watanabe, K. Ioku, J. Ceram. Soc. Jpn. 117 (2009) 385.
[24] A. Harada, S. Ban, N. Arimoto, M. Hattori, K. Narita, J. Hasegawa, Bioceramics 9 (1996) 325.
[25] W.L. Suchanek, K. Byrappa, R.E. Shuk, R. Pavel, V.F. Janas, K.S. Tenhuisen, Biomaterials 25 (2004) 4647.
[26] N. Kanzaki, K. Onuma, G. Treboux, S. Tsutsumi, A. Ito, J. Phys. Chem. B 104 (2000) 4189.
[27] G.N. Karanikolos, J.W. Wydra, J.A. Stoeger, H. García, A. Corma, M. Tsapatsis, Chem. Mater. 19 (2007) 792.
[28] K. Govender, D.S. Boyle, P.B. Kenway, P. O'Brien, J. Mater. Chem. 14 (2004) 2575.
[29] B.O. Fowler, Inorg. Chem. 13 (1974) 194.
[30] S. Ban, S. Maruno, N. Arimoto, A. Harada, J. Hasegawa, J. Biomed. Mater. Res. 36 (1997) 9.
[31] K. Yamashita, N. Oikawa, T. Umegaki, Chem. Mater. 8 (1996) 2697.
[32] O. Masataka, K. Mihoko, N. Satoshi, Y. Kimihiro, Key Eng. Mater. 218–220 (2002) 249.
[33] H. McDowell, T.M. Gregory, W.E. Brown, J. Res. Nat. Bur. Stand. A Phys. Chem. 81 (1977) 273.
[34] M. Mengiot, M.L. Harvill, O.R. Gilliam, J. Cryst. Growth 19 (1973) 199.
[35] M.J. Larsen, S.J. Jensen, Arch. Oral Biol. 34 (1989) 957.
[36] K. Ozeki, H. Aoki, T. Masuzawa, Appl. Surf. Sci. 256 (2010) 7027.
[37] P.W. Brown, J. Am. Ceram. Soc. 75 (1992) 17.
[38] F. Peters, M. Epple, J. Chem. Soc. Dalton Trans. (2001) 3585.